International Journal of Engineering

Numerical Investigation of Heat Transfer and Pressure Drop in a Corrugated Channel

H. M. Deylami, N. Amanifard*, M. Sanaei, R. Kouhikamali

Department of Mechanical Engineering, Faculty of Engineering, University of Guilan, P.O. Box 3756, Rasht, Iran

P A P E R   I N F O

A B S T R A C T

Changes in rib-height to channel-height ratio (e/H) has a significant effect on the heat transfer and pressure drop characteristics inside corrugated channels. In current paper, the variation of (e/H) was investigated numerically as well as a deep concern for finding the adequate turbulent model. In this regards, the governing equations were solved by a finite volume approach in a wide range of rib-height to channel-height ratio ($0.06 < e/H < 0.26$) and the Reynolds numbers ($5400 < Re < 23000$). The predicted results reveal that the RNG $k-\varepsilon$ turbulence model provides better agreement with available experimental data than other turbulence models. The computed results not only confirm the noticeable effects of (e/H) on the heat transfer performance and pressure drop but also, demonstrate the optimum corrugation design limits.

1. INTRODUCTION

Corrugated channels play a great role in heating and cooling systems. One of the most significant passive ways to improve the performance of the heat exchangers is using the corrugated channels instead of the flat plates. The heat transfer efficiency depends on a wide range of effective parameters in channels, and comprehensive reviews have been done in the two last decades. Sparrow et al. [1, 2] carried out an experimental work to determine the local and average heat transfer characteristics for flow in a triangular corrugated channel. They revealed that the average heat transfer coefficient has a significant growth for corrugated channel. An experimental study of convective heat transfer in a turbulent regime for a wavy wall channel with seven corrugations carried out by Saniei et al. [3]. They results showed that although the local Nusselt number distribution has the highest magnitude on the second wave, it followed the same pattern for all seven corrugations. Islamoglu et al. [4, 5] numerically and experimentally studied the effect of channel height on the heat transfer characteristics in a heat exchanger with corrugated channels. They demonstrated that the Nusselt number increases with an increment in the channel height in the same manner as

friction factor. In addition, Naphon et al. [6-8] experimentally and numerically studied the heat transfer and pressure drop characteristics in one-side and both-side corrugated channels with different tile angles and channel heights lied in inline and staggered arrays under constant heat flux. The obtained results showed that the corrugated surface has significant effect on the enhancement of heat transfer. Therefore, using corrugated plates is a proper method to increase the thermal performance and higher compactness of the heat exchanger. Elshafei et al. [9] performed experimental studies on the heat transfer and pressure drop in corrugated channels under uniform wall temperature with different cases of spacing and phase shifting. Their results showed that the variation in phase shift has not a significant effect on the friction factor compared to the effect of spacing variation, especially at higher Reynolds numbers. Eiamsa-ard et al. [10] utilized four different turbulence models in their numerical study on turbulent flow in a channel over periodic square grooves. They found that among different turbulence models, the RNG and standard $k-\varepsilon$ turbulence models generally provide higher accuracy agreements with available measurements data. Finally, they found that the grooved channel provides a considerable increase in heat transfer. Thianpong et al. [11] experimentally studied the influence of Reynolds number, rib height and ribs arrangement of turbulent

* Corresponding author email: *namanif@guilan.ac.ir* (N. Amanifard)

flow on the heat transfer and friction loss in a channel with isosceles triangular ribs. They revealed that the in line rib arrangement provides higher heat transfer and makes more friction loss than the staggered one. In addition, they exposed increasing the rib height with in line array causes to increase the Nusselt number and the friction factor values. A numerical investigation of heat transfer and pressure drop in three-dimensional geometries with the alternated opposed ribs has been carried out by T. Desrues [12]. The results indicate that the heat transfer enhances only when the Reynolds number is greater than a critical value. Tanda [13] performed an experimental study on the thermal performance in a rectangular channel with angled rib inclined at 45° on one or two surfaces of the channel. The results reveal that superior heat transfer performance occurs at the optimal rib pitch-to-height ratio of 13.33 for the one-ribbed wall channel and at 6.66–10 for the two-ribbed wall channel. The effect of amplitude of the waviness and the Reynolds number in a wavy wall channel was studied numerically by Ramgadia et al. [14]. They depicted that the critical Reynolds number of unsteadiness is dependent on the geometrical parameters and the geometry with H_{min}/H_{max} (minimum-to-maximum distance between plates) ratio equal to 0.2 produces the highest Nusselt number and the best thermal performance factor. In addition, Pashaie et al. [15] developed an adaptive Neuro-Fuzzy inference system (ANFIS) to estimate the Nusselt number along a wavy wall in a lid-driven cavity under mixed convection regime. Regarding to the mentioned literature reviews, the ribs configuration plays an important role in heat transfer and pressure drop evaluations in corrugated channels. The main goal of the current work is twofold. The first is to illustrate the influence of rib-height to channel-height ratio (e/H) on the heat transfer, friction factor and thermal enhancement characteristics in order to achieve higher efficiency for the corrugated channel. The second is to gain more reliable and faster solutions. In this way, four different types of turbulent models are being compared to each other, and a more suitable one is chosen for further studies.

2. GOVERNING EQUATIONS

The mass, momentum and energy equations are as follows:

$$\frac{\partial}{\partial x_i}(\rho u_i) = 0 \tag{1}$$

$$\frac{\partial}{\partial x_j}(\rho u_i u_j) = -\frac{\partial p}{\partial x_i}$$
$$+ \frac{\partial}{\partial x_i}\left[\mu\left(\frac{\partial u_i}{\partial x_j} + \frac{\partial u_j}{\partial x_i} - \frac{2}{3}\delta_{ij}\frac{\partial u_k}{\partial x_k}\right)\right] + \frac{\partial}{\partial x_j}(-\rho\overline{u_i' u_j'}) \tag{2}$$

$$\frac{\partial}{\partial x_j}(\rho u_j T) = \frac{\partial}{\partial x_i}\left((\Gamma + \Gamma_t)\frac{\partial T}{\partial x_i}\right) \tag{3}$$

where, Γ and Γ_t are molecular thermal diffusivity and turbulent thermal diffusivity, respectively, and are given by: $\Gamma = \frac{\mu}{Pr}$ and $\Gamma_t = \frac{\mu_t}{Pr_t}$

One of the most common methods, which is employed to relate the Reynolds stresses to the mean velocity gradients, is the Boussinesq hypothesis:

$$-\rho\overline{u_i' u_j'} = \mu_t\left(\frac{\partial u_i}{\partial x_j} + \frac{\partial u_j}{\partial x_i}\right) - \frac{2}{3}\left(\rho k + \mu_t\frac{\partial u_i}{\partial x_i}\right)\delta_{ij} \tag{4}$$

The advantage of this approach is the relatively low computational cost associated with the computation of the turbulent viscosity (μ_t) that is computed as a function of k and ε[1]. In order to gain to a more precise prediction, the predictive ability of four different turbulence models has been investigated: the standard $k-\varepsilon$, the Renormalized group (RNG) $k-\varepsilon$, the Low Reynolds $k-\varepsilon$ and the SST $k-\omega$ turbulence models. As shown in the section 5.1, the errors are minimal for the average Nusselt number and the friction factor when the RNG $k-\varepsilon$ model is used and results are well approved with the experimental data [10]. Equation (5) is a general tensor form in the Cartesian coordinates which governs the turbulence kinetic energy (k) and the turbulence dissipation rate (ε) equations for the RNG $k-\varepsilon$ model, with the specific values of φ, ψ and b which are listed in Table 1.

$$\frac{\partial(\rho u_i \varphi)}{\partial x_i} = \frac{\partial}{\partial x_i}\left(\psi\frac{\partial \varphi}{\partial x_i}\right) + b \tag{5}$$

3. NUMERICAL STUDY

3. 1. Objective Factors   The Reynolds number based on the hydraulic diameter of the channel is given by:

$$Re = UD/\nu \tag{6}$$

where, U is mean air velocity of the channel.
The friction factor is evaluated by:

$$f = \frac{2}{(L/D)}\frac{\Delta P}{\rho U^2} \tag{7}$$

where, ΔP is the pressure drop across the test section. The local heat transfer coefficient is used to investigate the heat transfer, which is defined as follows:

$$h_x = \frac{q''}{(T_{sx} - T_b)} \tag{8}$$

---

[1] Fluent 6.2 User's Guide, Fluent Inc., (2007)

TABLE 1. Summary of the equations solved for the RNG $k - \varepsilon$ turbulence model.

Equation	φ	ψ	b
Turbulence kinetic energy	k	$\alpha_k \mu_{eff}$	$G_k - \rho\varepsilon$
Turbulence dissipation rate	ε	$\alpha_\varepsilon \mu_{eff}$	$(C_{1\varepsilon}G_k - C_{2\varepsilon}^* \rho\varepsilon)\dfrac{\varepsilon}{k}$
For the turbulence kinetic energy equation:	$G_k = -\rho \overline{u_i' u_j'} \dfrac{\partial u_j}{\partial x_i}$ $\mu_{eff} = \mu + \mu_t$		$\mu_t = \rho C_\mu \dfrac{k^2}{\varepsilon}$
For the turbulence dissipation rate equation:	$C_{2\varepsilon}^* = C_{2\varepsilon} + \dfrac{C_\mu \eta^3(1 - \eta/\eta_0)}{1 + \beta\eta^3}$ $\eta = Sk\big/\varepsilon$ $\left\|\Omega_{ij}\right\| = \sqrt{2\Omega_{ij}\Omega_{ij}}$ $\left\|S_{ij}\right\| = \sqrt{2S_{ij}S_{ij}}$		$S \equiv \left\|\Omega_{ij}\right\| + C_p \min(0, \left\|S_{ij}\right\| - \left\|\Omega_{ij}\right\|)$ $\Omega_{ij} = \dfrac{1}{2}(\partial u_i\big/\partial x_j - \partial u_j\big/\partial x_i)$ $S_{ij} = \dfrac{1}{2}(\partial u_i\big/\partial x_j + \partial u_j\big/\partial x_i)$
Constants:	$C_{1\varepsilon} = 1.42$ $\eta_0 = 4.38$ $C_\mu = 0.0845$ $\alpha_k \approx 1.393$		$C_{2\varepsilon} = 1.68$ $\beta = 0.012$ $C_p = 2.0$ $\alpha_\varepsilon \approx 1.393$

where, T_{sx} is the local wall temperature.

The air bulk temperature between the inlet and outlet of the test section is given by the following relation:

$$T_b = \frac{T_{out} + T_{in}}{2} \tag{9}$$

Therefore, the average heat transfer coefficient is expressed by:

$$\overline{h} = \frac{q''}{(\overline{T_s} - T_b)} \tag{10}$$

The local and average Nusselt numbers are defined by the following equations:

$$Nu_x = \frac{h_x D}{K} \tag{11}$$

$$\overline{Nu} = \frac{\overline{h} D}{K} \tag{12}$$

It should be mentioned that all of thermo-physical properties of the air are determined at the bulk air temperature.

Thermal enhancement factor at equal pumping power is defined as the ratio of the convective heat transfer coefficient of the corrugated channel to that of the smooth one, which with consideration of relationship between friction factor and Reynolds number can be easily expressed as:

$$\eta = (\overline{Nu_c}\big/\overline{Nu_0})\big/(f_c/f_0)^{1/3} \tag{13}$$

3. 2. Boundary Conditions   At the inlet, velocity has been set based on the Reynolds number. Furthermore, values of k and ε for the inlet have been obtained from the terms of Equations (14) and (15).

$$k = \frac{3}{2}(UI)^2 \tag{14}$$

$$\varepsilon = C_\mu^{3/4} k^{3/2} l^{-1} \tag{15}$$

in which, I and l are calculated from the following relations:

$$I = 0.16 Re^{-1/8} \tag{16}$$

$$l = 0.07 \, D \tag{17}$$

The temperature at the inlet was set to 300K that is almost equal to room temperature. At the outlet of the domain, the fluid discharges to the atmosphere pressure; so the pressure gradient is equal to zero:

$$\left.\frac{\partial p}{\partial x}\right|_{exit} = 0 \tag{18}$$

No slip boundary condition is assumed for the both upper and lower plates. The upper wall is subjected to a uniform heat flux condition while the lower wall is isolated.

3. 3. Solution Procedure   FLUENT 6.3 as a commercial CFD software was used to perform all numerical simulations. The two-dimensional, incompressible time-independent Navier–Stokes equations and the turbulence model equations are discretized using the finite volume method. For the momentum equations, the pressure and velocities are linked together based on the SIMPLE algorithm of Patankar et al. [16] and profited analytically derived differential formula for effective viscosity. For near-wall modeling, enhanced wall treatment was implemented. The relaxation factors are set to 0.3 and 0.7 for the pressure and momentum correction equations, respectively and 0.8 for both of turbulent kinetic energy (k) and turbulent dissipation rate (ε) equations. The iterative procedure for all equations is terminated when the normalized continuity, energy, and turbulence residuals nowhere exceeded the value of 10^{-6}. On the other hand, the mass and energy balances as the convergence criteria have been checked after each solution.

3. 4. Grid Generation   To gain to an efficient grid, an integration of structured and unstructured meshes has been used, as shown in Figure 1a. As shown in Figures 1b and 1c, the grids have been clustered near the walls, where the appearance of more representative gradients is expected. In order to obtain the satisfactory solutions with the RNG $k-\varepsilon$ turbulent model, the grid independence is carried out for five different grid distributions. The predicted results of local heat transfer and skin-friction coefficients for different grid sizes are presented in Figure 2. In this figure, it is depicted that the grid distribution with 179106 cells nearly matches with those obtained by grid with 264076 cells for both h_x and ReC_f. In the other words, further increases for about 50% in cells causes less than 2% variation in local

heat transfer coefficient and 1.5% variation in skin-friction coefficient values. In consequence, the mesh with 179106 cells is more reliable.

4. GEOMETRIC CONFIGURATION

The schematic view of the complete domain used for the numerical simulation is shown in Figure 3.

The computational domain has a 20H length at entrance of the duct before test section in order to provide a hydro-dynamically fully developed flow and 10H length after the test section eliminates the exit effects (see Figure 3). The dimension of the test section is the same as the corrugated channel of Thianpong et al. [10]. The test section is located in the middle part of the duct that includes ten uniform periodic corrugated ribs with inline array - peak to peak - along both upper and lower channel walls. The geometric characters of the channel are described in Table 2.

TABLE 2. Geometric parameters.

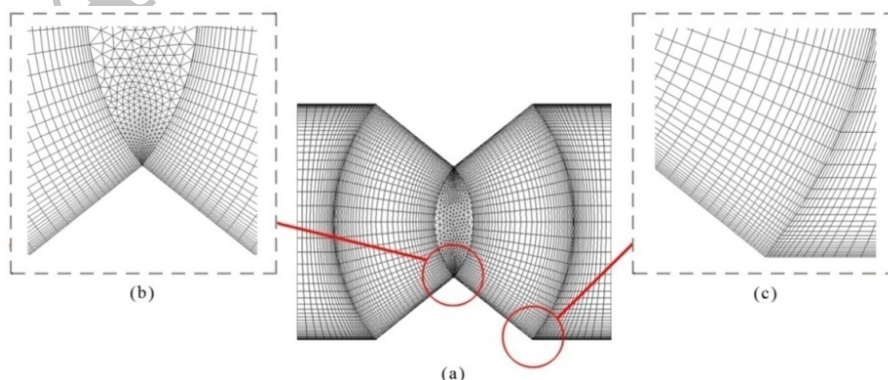| Parameter	Value (mm)
Channel overall length	1340
Channel height, H	30
Channel wide, W	300
Test Section length, L	440
Downstream length	600
Upstream length	300
Rib height, e	2,4,6,8
Rib thickness, t	40
Axial length of each cycle or pitch, P	40

Figure 1. Schematic grid arrangement for the corrugated channel
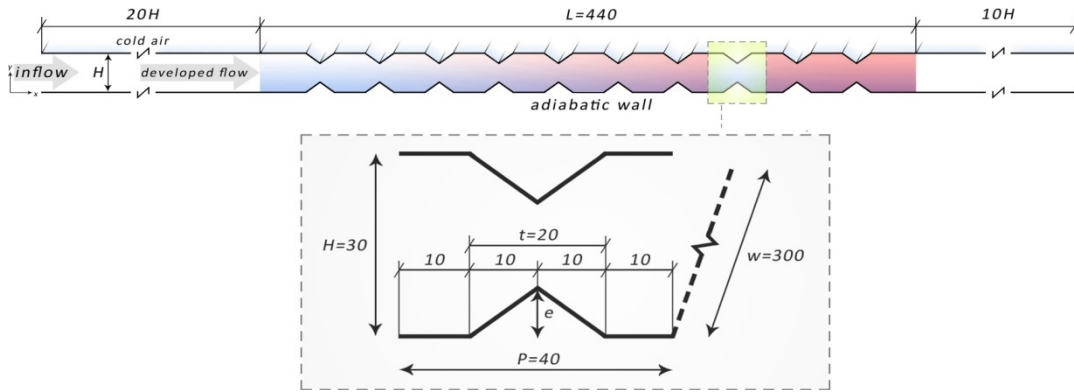
Figure 3. Schematic view of the complete numerical domain.
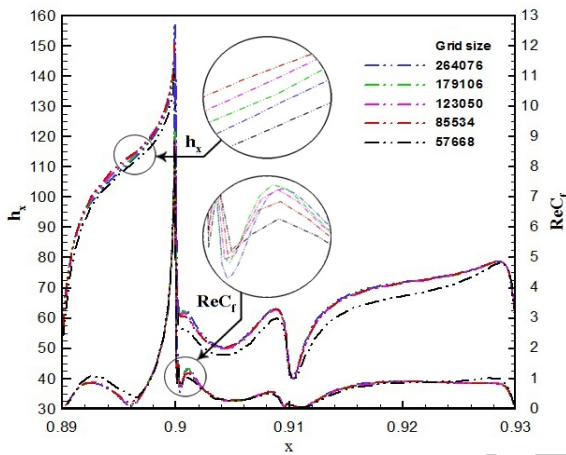

Figure 2. The effect of grid densities on local convective heat transfer coefficient and skin-friction coefficient for eighth rib at Re = 23000.
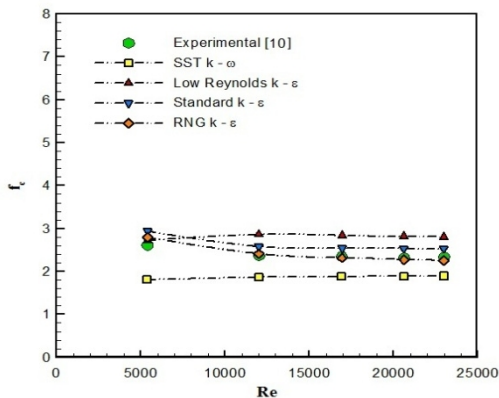

Figure 4. The comparison between friction factors for different turbulent models.

5. RESULTS AND DISCUSSIONS

The influence of variation in rib-height to channel-height ratio (e/H) on the heat transfer, the friction loss,

and the efficiency of the channel in different Reynolds numbers was investigated in this study. The corrugated channels with four different rib heights of 2, 4, 6, 8 and for Reynolds number in the range of 5400-23000 were tested. In order to approve the accuracy of a numerical investigation, the computed results have been evaluated in comparison with the available experimental data.

5. 1. Effect of Turbulence Models   Figures 4 and 5 show the variations of friction factor and average Nusselt number with Reynolds number for different turbulence models. It is clear that the most adequate results belong to the RNG $k-\varepsilon$ model. The values obtained from this model are consistent with the experimental data and lie within error -4% to +7% for the friction factor and -10% to +7% for the average Nusselt number as illustrated in Figure 6. The mean relative error (MRE) for this model is also 7.42% for $\overline{Nu_c}$ and 3.02% for f_c. The error indicates the maximum deviation of the predicted values from the experimental data and it is given with the following mathematical definition:

$$error = \frac{(p_i - m_i)}{m_i} \times 100 \tag{19}$$

and MRE is calculated according to the following expression:

$$MRE = \frac{100}{n} \sum_{i=1}^{n} \frac{|p_i - m_i|}{m_i} \tag{20}$$

where, m_i is experimentally measured value, p_i is numerically predicted value and n is the number of data. In addition, after RNG $k-\varepsilon$ model, the standard $k-\varepsilon$ model with the error less than 12% for both $\overline{Nu_c}$ and f_c, has an adequate agreement with the experimental data. Furthermore, the computed results are under-estimated in the case SST $k-\omega$ model and they are over-estimated in the case of Low Reynolds $k-\varepsilon$

model. It is noticeable that Low Reynolds $k-\varepsilon$ turbulence model gives a higher accuracy in lower Reynolds numbers and the error of this model grows with increasing Reynolds number for both of average Nusselt number and friction factor.
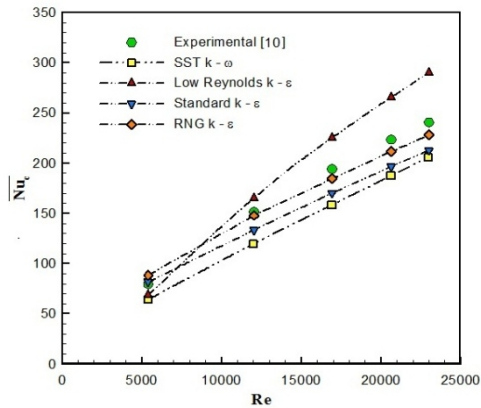

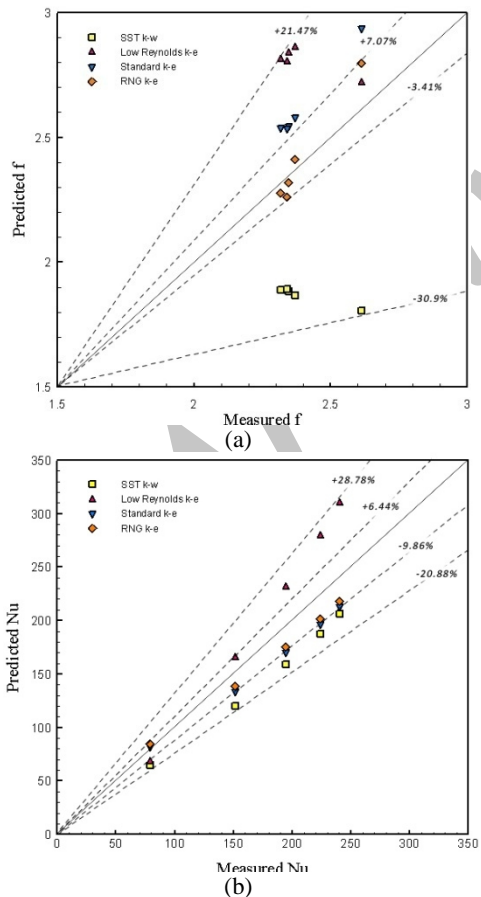**Figure 5.** The comparison between average Nusselt numbers for different turbulent models.

(a)

(b)

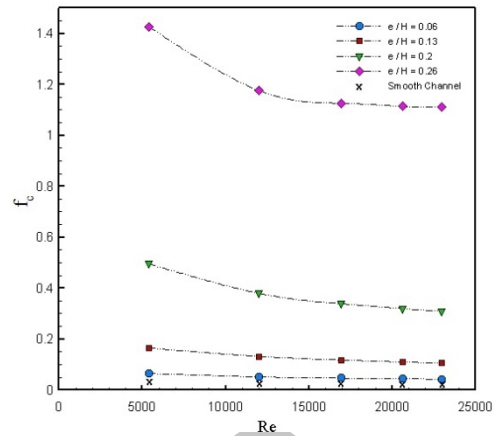**Figure 6.** Experimental measured f_c versus numerical predicted f_c (a) and measured $\overline{Nu_c}$ versus numerical predicted $\overline{Nu_c}$ (b).

Figure 7. The effect of variation in the Reynolds number and e/H on friction factor, f_c.
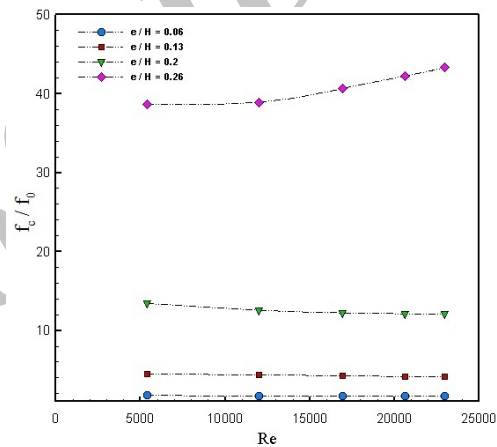
Figure 8. The effect of variation in the Reynolds number and e/H on friction factor ratio, f_c/f_0.

5. 2. Effect of Rib Height   As shown in Figure 7, with increasing e/H, friction factor increases. This reality relates to the increase of swirl flow zones and increase of the angle of triangle rib (θ), and consequently, the drag forces exerted on the flow field by the corrugated surface. As shown in Figure 8, the values of f_c/f_0 decreases gently with increasing Reynolds except for e/H = 0.26. As can be perceived from the curves in the Figure 8, for a wide range of Reynolds, increasing e/H fairly after 0.2 (e = 6), causes a significant pressure drop penalty and leads to poor performances of corrugations with rib-height to channel-height ratio (e/H) over than 0.2. As it is depicted in Figures 9 and 10, increasing e/H causes a significant increase in $\overline{Nu_c}$, and $\overline{Nu_c}/Nu_0$. For instance, increasing e/H from 0.13 to 0.26, makes 46% increment in $\overline{Nu_c}/Nu_0$ because of higher disturbance and increment in heat transfer surface up to 5.1%. Figure 11 shows the effect of variation in the Reynolds number and e/H on the thermal enhancement factor.
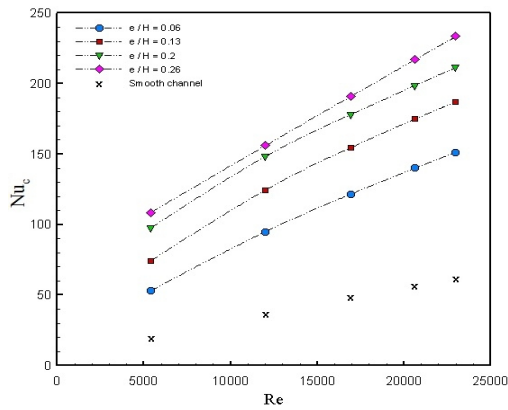
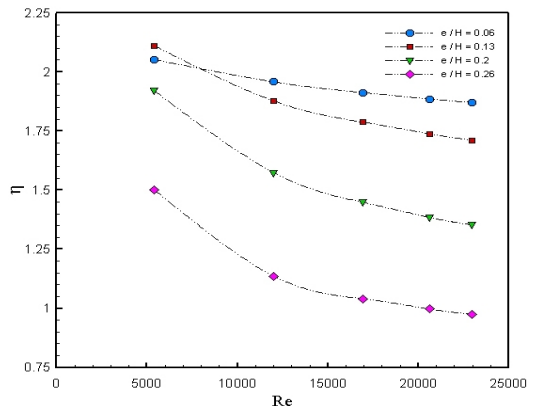**Figure 9**. The effect of variation in the Reynolds number and e/H on the average Nusselt number, $\overline{Nu_c}$.

Figure 11. The effect of variation in the Reynolds number and e/H on the thermal enhancement factor.
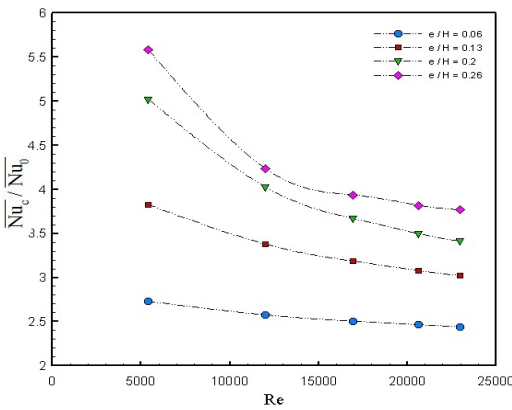

Figure 10. The effect of variation in the Reynolds number and e/H on average Nusselt number ratio, $\overline{Nu_c}/\overline{Nu_0}$.

As shown in this figure, increasing the e/H decreases the efficiency of channel. Although the configuration of e/H = 0.06 has the lowest $\overline{Nu_c}$ but it has the highest efficiency. This originates from lower friction factors as a result of small swirl flow zones when compared to the other values of e/H.

As shown in Figure 12, since swirl zones and disturbance grow with increasing e/H, the maximum Nusselt number belongs to highest Reynolds number for all selected channels.
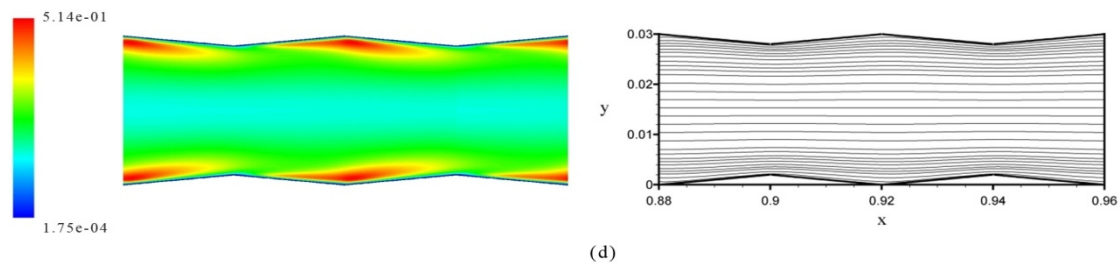

(a)

(b)

(c)
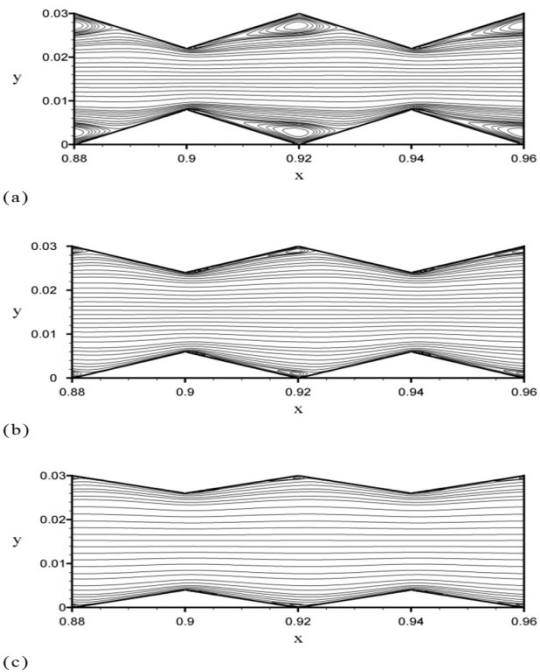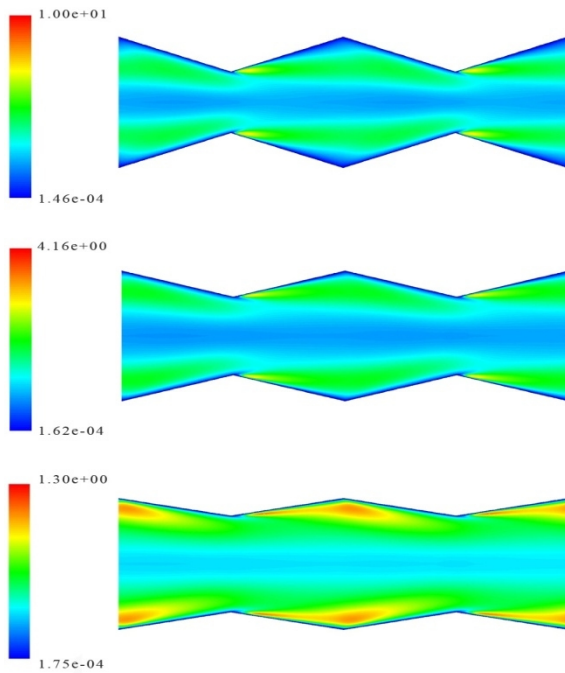
Figure 12. Contour plots of turbulence kinetic energy (left column) and stream function (right column) of eighth and ninth ribs at (a) e/H = 0.26, (b) e/H = 0.2, (c) e/H = 0.13 and (d) e/H = 0.06.

5. CONCLUSION

The effect of using different profiles of corrugated channels on the heat transfer and friction characteristics were numerically investigated, and the average Nusselt number, friction factor and the thermal enhancement factor were set as the objectives to evaluate the effectiveness of the corrugated channels. The computed results may interpret the following conclusions:

Comparison of predicted results using different tested turbulence models with experimental data shows that the RNG $k-\varepsilon$ turbulence model is the most accurate model for predicting heat transfer and pressure drop over periodic corrugated double side channels. On the other hand, increasing the rib-height ratio (e/H) increases the friction factor. Increasing e/H from 0.2 to 0.26 cause noticeable increasing in f_c when compared to the cases with variation of e/H from 0.13 to 0.2. This trend highlights the reality of significant nonlinear dependency of e/H to objective parameters and vice versa. The changes between 0.2 and 0.13 show the start zone of significant variation. Increasing e/H also causes a significant increase of $\overline{Nu_c}$. The heat transfer enhancement is obtained up to 144% - 173%, 202% - 282%, 241% - 402% and 277% - 458% in the cases of e/H is equal to 0.06, 0.13, 0.2 and 0.26, respectively (t/P = 1) in the Reynolds number range of 5400 - 23000. Morover, Increasing Reynolds number and the rib-height to channel-height ratio (e/H) cause decreasing in η.

6. REFERENCES

1. Goldstein Jr, L. and Sparrow, E., "Heat/mass transfer characteristics for flow in a corrugated wall channel", *ASME Transactions Journal of Heat Transfer*, Vol. 99, (1977), 187-195.
2. O'Brien, J. E., "Corrugated duct heat transfer, pressure drop and flow visualization", *Transactions of the ASME, Journal of Heat Transfer*, Vol. 104, (1982), 410-416.
3. Saniei, N. and Dini, S., "Heat transfer characteristics in a wavy-walled channel", *Journal of Heat Transfer*, Vol. 115, No. 3, (1993), 788-792.
4. Islamoglu, Y. and Parmaksizoglu, C., "The effect of channel height on the enhanced heat transfer characteristics in a corrugated heat exchanger channel", *Applied Thermal Engineering*, Vol. 23, No. 8, (2003), 979-987.
5. Islamoglu, Y. and Parmaksizoglu, C., "Numerical investigation of convective heat transfer and pressure drop in a corrugated heat exchanger channel", *Applied Thermal Engineering*, Vol. 24, No. 1, (2004), 141-147.
6. Naphon, P., "Heat transfer characteristics and pressure drop in channel with v corrugated upper and lower plates", *Energy Conversion and Management*, Vol. 48, No. 5, (2007), 1516-1524.
7. Naphon, P. and Kornkumjayrit, K., "Numerical analysis on the fluid flow and heat transfer in the channel with v-shaped wavy lower plate", *International Communications in Heat and Mass Transfer*, Vol. 35, No. 7, (2008), 839-843.
8. Naphon, P., "Effect of corrugated plates in an in-phase arrangement on the heat transfer and flow developments", *International Journal of Heat and Mass Transfer*, Vol. 51, No. 15, (2008), 3963-3971.
9. Elshafei, E., Awad, M., El-Negiry, E. and Ali, A., "Heat transfer and pressure drop in corrugated channels", *Energy*, Vol. 35, No. 1, (2010), 101-110.
10. Eiamsa-ard, S. and Promvonge, P., "Numerical study on heat transfer of turbulent channel flow over periodic grooves", *International Communications in Heat and Mass Transfer*, Vol. 35, No. 7, (2008), 844-852.
11. Thianpong, C., Chompookham, T., Skullong, S. and Promvonge, P., "Thermal characterization of turbulent flow in a channel with isosceles triangular ribs", *International Communications in Heat and Mass Transfer*, Vol. 36, No. 7, (2009), 712-717.
12. Desrues, T., Marty, P. and Fourmigué, J., "Numerical prediction of heat transfer and pressure drop in three-dimensional channels with alternated opposed ribs", *Applied Thermal Engineering*, (2012).
13. Tanda, G., "Effect of rib spacing on heat transfer and friction in a rectangular channel with 45° angled rib turbulators on one/two walls", *International Journal of Heat and Mass Transfer*, Vol. 54, No. 5, (2011), 1081-1090.
14. Ramgadia, A. G. and Saha, A. K., "Fully developed flow and heat transfer characteristics in a wavy passage: Effect of amplitude of waviness and reynolds number", *International Journal of Heat and Mass Transfer*, Vol. 55, No. 9, (2012), 2494-2509.
15. Pashaie, P., Jafari, M., Baseri, H. and Farhadi, M., "Nusselt number estimation along a wavy wall in an inclined lid-driven cavity using adaptive neuro-fuzzy inference system (anfis)", *International Journal of Engineering-Transactions A: Basics*, Vol. 26, No. 4, (2012), 383.
16. Patankar, S. V. and Spalding, D. B., "A calculation procedure for heat, mass and momentum transfer in three-dimensional parabolic flows", *International Journal of Heat and Mass Transfer*, Vol. 15, No. 10, (1972), 1787-1806.

Numerical Investigation of Heat Transfer and Pressure Drop in a Corrugated Channel

H. M. Deylami, N. Amanifard, M. Sanaei, R. Kouhikamali

Department of Mechanical Engineering, Faculty of Engineering, University of Guilan, P.O. Box 3756, Rasht, Iran

چکیده

در تحقیق حاضر، به بررسی عددی تاثیر نسبت ارتفاع پره ها به ارتفاع کانال بر روی مشخصه های انتقال حرارت و افت فشار در یک کانال چین دار تحت شرایط دو بعدی، آشفته، غیر قابل تراکم و پایا پرداخته شده است. مسئله مورد نظر برای محدوده گسترده ای از نسبت ارتفاع پره به ارتفاع کانال (۰/۲٦ ≥ H / e ≥ ۰/۰ ٦) و اعداد رینولدز (۲۳۰۰۰ > Re < ٥٤۰۰) با روش حجم محدود مورد تحلیل قرار گرفته است. نتایج نشان می دهند که تغییر این پارامتر تاثیر قابل توجهی بر روی انتقال حرارت، افت فشار و ضریب عملکرد کانال دارد. همچنین به جهت تشخیص تاثیر مدل آشفتگی مورد استفاده در نتایج بدست آمده و یافتن بهترین مدل، چهار مدل آشفتگی متفاوت مورد بررسی قرار گرفته است. نتایج حاکی از آن است که در تحلیل جریان سیال در چنین کانالهایی، مدل آشفتگی RNG k – ε بیشترین مطابقت را با نتایج آزمایشی داراست.

doi: *10.5829/idosi.ije.2013.26.07a.12*